Spectra and Scattering of Light Lattice Nuclei from Effective Field Theory

J. Kirscher,[1] N. Barnea,[1] D. Gazit,[1] F. Pederiva,[2,3] and U. van Kolck[4,5]

[1]*Racah Institute of Physics, The Hebrew University, Jerusalem 91904, Israel*
[2]*Physics Department, University of Trento, via Sommarive 14, I-38123 Trento, Italy*
[3]*INFN-TIFPA Trento Institute for Fundamental Physics and Applications, Trento, Italy*
[4]*Institut de Physique Nucléaire, CNRS/IN2P3, Université Paris-Sud, F-91406 Orsay, France*
[5]*Department of Physics, University of Arizona, Tucson, AZ 85721, USA*

(Dated: July 11, 2018)

An effective field theory is used to describe light nuclei, calculated from quantum chromodynamics on a lattice at unphysically large pion masses. The theory is calibrated at leading order to two available data sets on two- and three-body nuclei for two pion masses. At those pion masses we predict the quartet and doublet neutron-deuteron scattering lengths, and the alpha-particle binding energy. For m_π=510 MeV we obtain, respectively, ${}^4a_{\mathrm{nD}} = 2.3 \pm 1.3$ fm, ${}^2a_{\mathrm{nD}} = 2.2 \pm 2.1$ fm, and $B_\alpha = 35 \pm 22$ MeV, while for m_π=805 MeV ${}^4a_{\mathrm{nD}} = 1.6 \pm 1.3$ fm, ${}^2a_{\mathrm{nD}} = 0.62 \pm 1.0$ fm, and $B_\alpha = 94 \pm 45$ MeV are found. Phillips- and Tjon-like correlations to the triton binding energy are established. Higher-order effects on the respective correlation bands are found insensitive to the pion mass. As a benchmark, we present results for the physical pion mass, using experimental two-body scattering lengths and the triton binding energy as input. Hints of subtle changes in the structure of the triton and alpha particle are discussed.

I. INTRODUCTION

The vast number of phenomena of the nuclear chart depend on a relatively small set of quantum chromodynamics (QCD) parameters — in the low energies relevant for nuclear physics, a mass scale $M_{\rm QCD}$ associated to the strong coupling constant, the masses m_q of the two lightest quarks, the electromagnetic coupling strength, and the vacuum angle. Lattice QCD (LQCD) is a numerical framework which enables us, at least in principle, to relate nuclear and QCD parameters, once effects due to finite lattice spacing and size are removed. The last few years have witnessed significant progress in predicting the properties of light nuclei with nucleon number $A \leq 4$, but at relatively large quark masses and neglecting time-reversal and isospin violation. (See Ref. [1] for a review and a list of relevant references).

Increasing A at fixed quark masses presents significant difficulties because the noise-to-signal rate increases exponentially. Although there seem to be ways around this problem [1], large A also requires that longer distances be covered by the lattice, since the nuclear volume increases with A. As in other areas of physics, it is profitable to change to a more effective description, in this case to an effective field theory (EFT) involving nucleons as degrees of freedom. Because an EFT is based on the most general Hamiltonian with the appropriate symmetries, it is guaranteed to produce S-matrix elements consistent with the S matrix of the underlying theory [3], here QCD. After matching the EFT amplitudes to the LQCD-calculated quantities at small A, one can describe the longer-distance dynamics involved in larger-A systems within the EFT [2], which is considerably simpler than doing so directly within LQCD.

Most LQCD results so far concern binding energies, but reactions convey much more information and will command increasing attention in the years to come. Unfortunately, as discussed in Ref. [4], which also summarizes the progress in this field, volume artifacts are more pronounced. EFT quite naturally accounts for scattering states, and allows bound states and scattering to be treated on equal footing. Here we elaborate on the findings of Ref. [2] for $A \leq 4$ and extend, for the first time, LQCD predictions to reactions involving nuclei. As an example, we consider neutron-deuteron (nD) scattering at low energies, where the two S-wave channels — with total spin $s = 3/2$ (quartet) and $s = 1/2$ (doublet) — are most important.

The noise-to-signal rate in LQCD also increases with decreasing m_q. Results obtained with unphysical m_q can, in principle, be extrapolated to the physical point in a systematic way using chiral effective field theory (χEFT), as long as pion masses are within the radius of convergence of the latter. From χEFT with up to one nucleon — that is, chiral perturbation theory (χPT) — one obtains the m_q dependence of, for example, the average pion mass (m_π) [8], and of the nucleon ($m_{\rm N}$) and Delta (m_Δ) masses [6]. The m_q dependence of some few-nucleon observables has also been estimated [7], but unfortunately significant uncertainties still exist due to subtleties in the proper accounting of renormalization-group (RG) invariance in this non-perturbative context [7, 56, 63].

The average pion mass m_π is commonly used as a measure for the detuned value of the average quark mass. At present, LQCD can be carried out in the meson and single-hadron sector down to values of m_π close to physical, where the low-lying mass spectrum is reproduced within theoretical error bars (see Ref. [12] for a status report). Comparison with LQCD data suggests that χPT converges for pion masses no larger than about 500 MeV [64]. In contrast, the quark masses employed in current nuclear LQCD are likely beyond reach of χEFT.

As proposed in Ref. [2] and elaborated here, the EFT that describes existing light-nuclear LQCD data need not include pions explicitly. In fact, it has been understood for over fifteen years that even at the physical pion mass light nuclei are well described by pionless EFT ($\not\pi$EFT), an EFT with non-relativistic nucleons interacting through contact forces with an increasing number of derivatives — each with a strength parameter or "low-energy constant" (LEC) — which contribute at increasing orders. In two-nucleon scattering, $\not\pi$EFT reproduces [13, 65–67] the effective range expansion (ERE): scattering lengths at leading order (LO), effective ranges at next-to-leading order (NLO), *etc.* It thus also gives two-nucleon binding momenta in the $^3S_1$ and $^1S_0$ with corresponding accuracy. More importantly, $\not\pi$EFT offers a consistent extension of the ERE to other systems [20]. For example, S-wave nD scattering in the quartet channel can be very accurately postdicted [16–20] once the two-nucleon LECs have been fixed in the two-nucleon system. In the doublet channel, in contrast, RG invariance requires that the three-body force with no derivatives appear already at LO, with isospin-symmetric corrections starting beyond NLO [16, 21–28]. Current evidence from the RG in the four-body system suggests that there is no four-body force up to NLO [29–32]. The existence of a single three-body parameter up to NLO, which determines the three- and higher-body spectra, leads to many correlations among few-body observables at fixed two-body input. Examples are the so-called Phillips [33] and Tjon [11] lines obtained in plots of the doublet nD scattering length [23, 24] and alpha-particle binding energy [29, 32] as functions of the triton binding energy. Higher partial waves in three-nucleon scattering [19, 34], four-nucleon scattering [36], and even ^{6}Li [35] can also be reasonably well described in $\not\pi$EFT.

We will show that an analogous approach to describe light nuclei is equally useful at larger m_π. Using higher-than-physical m_q not only increases m_π, but also changes the nucleon mass $m_{\rm N}$ and the masses of all other hadrons. We will argue on the basis of scales inferred from LQCD data that nucleons are sufficient for momenta up to m_π, with neither explicit pions nor other baryons. Whether it is indeed m_π (instead of, say, $m_\Delta - m_{\rm N}$) that determines the

convergence rate of the theory used here is the subject of an upcoming investigation. At each value of m_π a pionless EFT exists with specific values of the LECs; we refer to $\not\pi$EFT with varying m_π as $\not{\vec\pi}$EFT in the following. Until nuclear LQCD calculations are extended to include time-reversal and isospin violation, m_π is the only QCD parameter determining nuclear properties. Existing data at $m_\pi = 805$ [37] and 510 [38] MeV give $A \leq 4$ binding energies that are much larger than in the real world and increase with the pion mass. The dineutron is bound, which could signal qualitative new features in lattice worlds. An obvious question is the extent to which properties of $\not\pi$EFT survive in $\not{\vec\pi}$EFT, where all scales change.

In Ref. [2] the binding energies of nuclei with $A \leq 6$ were studied in LO $\not{\vec\pi}$EFT using as input the LQCD data for dineutron, deuteron and triton/helion at $m_\pi = 805$ MeV [37]. The alpha-particle binding energy provided a consistency check between $\not{\vec\pi}$EFT and LQCD data, and the $A = 5, 6$ binding energies obtained with $\not{\vec\pi}$EFT can be viewed as an extrapolation of LQCD. Here, we extend $\not{\vec\pi}$EFT to the $m_\pi = 510$ MeV LQCD data [38] and to a broader range of observables including scattering amplitudes.

The methods of $\not\pi$EFT have for some time been deployed in the study of reactions directly on the lattice [4, 40]. Both two-nucleon elastic scattering [39] and neutron radiative capture on the proton [41] have been considered directly on the lattice. Our strategy is, instead, to analyze reactions outside the lattice box with $\not{\vec\pi}$EFT once its LECs have been determined from binding energies at LO and, eventually, also two-nucleon scattering observables at NLO. We exploit the dramatic advances in the development of the so-called *ab initio* methods that have taken place in nuclear physics over the same period in which $\not\pi$EFT was formulated. In particular, here we employ the effective-interaction hyperspherical-harmonic (EIHH) method [42–44], and the refined resonating-group (ℝGM) method [69]. Although these methods have been developed for traditional nuclear potentials, they can be adapted to pionless EFT, as already done for $\not{\vec\pi}$EFT in the EIHH [2] and $\not\pi$EFT in the ℝGM [32, 36].

Thus, we show that $\not\pi$EFT remains useful in nuclear systems with $A \leq 4$ and extrapolate LQCD data to observables that might not be as easily obtained in the lattice. This is analogous to the use of $\not\pi$EFT correlations [45, 46] to infer values of poorly measured observables in the real world. If and when scattering observables are determined directly on the lattice, our predictions will be a further test of the consistency between $\not{\vec\pi}$EFT and LQCD, establishing the validity of a theory with only contact interactions over a range of m_π from 140 MeV up to 805 MeV. Such a consistency would provide a benchmark for the extension of this method to the less-understood χEFT, once LQCD data reaches sufficiently small pion masses.

We summarize the article as follows. In Sec. II we discuss the degrees of freedom and breakdown scale of $\not{\vec\pi}$EFT for m_π up to ~ 800 MeV. Still in Sec. II, we present the LO Hamiltonian and the regulator we use in calculations, which employ the computational tools introduced in Sec. III: the EIHH and ℝGM methods. In Sec. IV, we determine the LO LECs from the LQCD data for $A \leq 3$ in the alternate reality assessed via LQCD at various m_π. With the Hamiltonian thus calibrated, we calculate in Sec. V the alpha-particle binding energy, establish the heavy pion Phillips and Tjon lines, and predict the doublet and quartet neutron-deuteron scattering lengths $^2a_{\mathrm{nD}}$ and $^4a_{\mathrm{nD}}$. As we conclude in Sec. VI the procedure is analogous to the development of $\not\pi$EFT over the last decades, namely, a calibration of a small set of parameters to data in order, first, to obtain predictions of low-energy observables and, second, to explain correlations amongst them.

II. PIONLESS EFFECTIVE FIELD THEORY

At physical m_π, pionless EFT with nucleons as the sole degrees of freedom has proved useful for light nuclei in the low-momentum regime — see Refs. [47, 48] for reviews and Ref. [49] for a pedagogical introduction. Its organizational scheme ("power counting") is based on two basic scales: the breakdown scale Q_{high} estimated as m_π and an unnaturally small scale $\aleph$ related to the inverse of the two-nucleon scattering lengths $^{1,3}a_{\mathrm{NN}}$ in the singlet/triplet channels.

For external relative momenta $k \lesssim m_\pi/2$, the deuteron and the virtual singlet bound state are the only singularities of the two-body scattering amplitude. All mesons and excited baryons are short-range effects. The amplitude from a Lagrangian built of derivative contact operators made of nucleon fields can be matched to all orders of the ERE. Matching the LO amplitude to the ERE results in a $C_{s,t} \propto 4\pi(^{1,3}a_{\mathrm{NN}})/m_{\mathrm{N}} \sim 4\pi/(m_{\mathrm{N}}\aleph)$ scaling of the non-derivative four-nucleon contact term. As the scattering lengths $^{1,3}a_{\mathrm{NN}}$ are large relative to the pion range $1/m_\pi$ for both NN S-wave channels, a refined power counting is required [65, 66] that goes beyond naive dimensional analysis. Of course, care has to be taken that the necessary regularization and the inclusion of higher-order contributions do not introduce poles within the radius of convergence. As long as those singularities are beyond the pion threshold, m_π, $\not\pi$EFT converges for two-nucleon processes at momenta $Q < Q_{\mathrm{high}}$, including the $^3S_1$ (deuteron) and $^1S_0$ poles [13, 67]. In LO the two LECs $C_{s,t}$ suffice.

Extending $\not\pi$EFT to systems with more nucleons requires understanding how $\aleph$ enters the LECs of multinucleon interactions. The fact that the non-derivative six-nucleon contact interaction is needed to define the EFT at LO [21, 22] implies its LEC scales as $D_d \sim (4\pi)^2/(m_{\mathrm{N}}\aleph^4)$. In contrast, the apparent lack of similar RG enhancements in

TABLE I. Relevant scales for a low-energy nuclear effective field theory. Physical data in the first column is relevant for ̸πEFT, lattice data summarized in the second and third for ̸πEFT. All numbers are given in MeV.

pion mass	m_π	139.5 ± 0.1 [72]	511 ± 2 [38]	806 ± 1 [37]
nucleon mass	m_N	$939 \pm 1, 938 \pm 1$ [74]	1320 ± 3 [38]	1634 ± 18 [37]
Delta-nucleon mass difference	$\delta_\Delta = m_\Delta - m_\mathrm{N}$	292 ± 1 [50]	≈ 200 [51]	≈ 180 [51]
dineutron binding energy	B_nn	—	7.4 ± 2 [38]	15.9 ± 4 [37]
deuteron binding energy	B_D	2.22 [52]	11.5 ± 2 [38]	19.5 ± 5 [37]
triton binding energy	B_T	8.482 [73]	20.3 ± 4.5 [38]	53.9 ± 10.7 [37]
inverse singlet scattering length	$^1a_\mathrm{np}^{-1}$	-8.31 [53]	n.a.	84.7 ± 18 [39]
inverse triplet scattering length	$^3a_\mathrm{np}^{-1}$	36.4 [53]	n.a.	108 ± 13 [39]
Delta effective momentum	$\sqrt{2m_\mathrm{N}\delta_\Delta}$	741	890	767
two-nucleon binding momentum	$\sqrt{m_\mathrm{N}(B_\mathrm{nn} + B_\mathrm{D})/2}$	46	112	170
triton-to-deuteron binding ratio	$B_\mathrm{T}/B_\mathrm{D}$	3.82	1.8	2.8

other contact interactions suggests they appear only in higher orders.

As ̸πEFT is applied beyond the deuteron, one needs to account for effects of the Coulomb force among protons. The importance of Coulomb effects is characterized by a ratio $\alpha m_N/Q$, where α is the fine-structure constant. Although crucial for very low-energy proton-proton [67] and proton-nucleus scattering, the Coulomb interaction should be subleading in relatively deep ground states such as helion and alpha particle, where binding momenta are much larger than αm_N.

At LO, the ̸πEFT Lagrangian can be written as

$$
\mathcal{L}_{LO} = N^\dagger \left(i\partial_0 + \frac{\vec{\nabla}^2}{2m_\mathrm{N}} \right) N + \frac{C_s}{8} \left(N^T \sigma^2 \sigma^i \tau^2 N \right)^\dagger \left(N^T \sigma^2 \sigma^i \tau^2 N \right) + \frac{C_t}{8} \left(N^T \sigma^2 \tau^2 \tau^a N \right)^\dagger \left(N^T \sigma^2 \tau^2 \tau^a N \right)
$$
$$
+ D_d (N^\dagger N)(N^\dagger N)(N^\dagger N), \tag{1}
$$

where N is a bi-spinor in both spin and isospin spaces, and σ^i (τ^a) are the spin (isospin) Pauli matrices, the index i (a) running over spin (isospin) vector components of the projection operators on the spin singlet (triplet) state. Higher orders contain terms with more derivatives and/or nucleon fields, including those necessary to ensure Lorentz invariance (in a Q/m_N expansion).

Somewhat surprisingly, ̸πEFT seems to converge for triton and helion [23, 24, 26], and even for the more-bound alpha particle [29, 32]. At the physical point, ̸πEFT is useful even at LO to explain features like correlations amongst three-body observables (the Phillips line) and between three- and four-body data (the Tjon line), with just the neutron-proton scattering lengths $^{1,3}a_\mathrm{np}$ as input. With an additional condition which conventionally fixes either the triton binding energy B_T or the neutron-deuteron doublet scattering length $^2a_\mathrm{nD}$, a few four-nucleon observables — e.g., the binding energy of ^{4}He [29, 32], and the neutron-triton and proton-helion scattering lengths [36] — have been found to agree with data within the expected uncertainty margin. The only exception so far seems to be the resonance location in the 0^- neutron-triton channel, which was found to be cutoff, and thus renormalization-scheme dependent [81]. The origin of this pathology is unknown. LO results for ^{6}Li [35] do not allow conclusions about the range in A where ̸πEFT converges.

With the usefulness at physical m_π thus established, we follow an analogous approach at heavier m_q. Available lattice data [12] identifies the pion, still, as the lightest meson and the Delta as the lowest excited state of the nucleon. However, the ratios between the nucleon, pion, and Delta masses change, see Table I. Also, nuclei become increasingly more bound.

The relevant momentum is very clear in the two-nucleon system, from either the inverse scattering lengths or the two-nucleon binding momentum estimated from the average two-nucleon binding energy. At all pion masses it is much smaller than the nucleon mass, meaning nucleons are nonrelativistic, and even than the pion mass itself, ensuring pions can be integrated out. However, in contrast to the physical world, $m_\pi > m_\Delta - m_\mathrm{N} \equiv \delta_\Delta$ for the two lattice simulations, and hence one might wonder if the Delta should not be included as an explicit degree of freedom.

The reason the Delta can still be integrated out is, of course, that in a nonrelativistic theory the relevant quantity for convergence is momentum, not heavy-particle mass. In this case, it is the "Delta effective momentum" $\sqrt{2m_\mathrm{N}\delta_\Delta}$, which remains above, or at least near, the pion mass. That $\sqrt{2m_\mathrm{N}\delta_\Delta}$ is the relevant scale was shown explicitly in Ref. [54] for the two-nucleon $^1S_0$ channel. In this case, the lowest accessible state with excitations has two Deltas, and in addition to C_s two other non-derivative contact interactions need to be included: two-nucleon/two-Delta and

four-Delta. Under the assumption that all three LECs are of a similar size C_0, they scale as [54]

$$C_0 = \frac{4\pi}{m_{\mathrm{N}}} \left({}^1a_{\mathrm{NN}}^{-1} + \sqrt{2m_{\mathrm{N}}\delta_\Delta} \right)^{-1} \approx (234 \text{ MeV})^{-2} \tag{2}$$

at m_π=140 MeV. Because the inverse value of the singlet scattering length for m_π=805 MeV, displayed in Table I, is about 10 times larger in magnitude than its physical analog, the ensuing size of C_0 would decrease and allow for higher typical momenta in the two-nucleon amplitude. However, the Delta effective momentum is still several times larger than the inverse scattering length. Operators in a Deltaful, pionless theory should then show similar scaling behavior as for physical pion mass, where the Delta can be integrated out. Removing the Delta generates an effective range not accounted for in LO, but this contribution is characterized by the Delta effective momentum, which does not seem to be smaller than the inverse pion mass.

This argument can be generalized to other channels [55] where $\sqrt{2m_{\mathrm{N}}\delta_\Delta}$ is replaced by $\sqrt{m_{\mathrm{N}}\Delta_{\mathrm{r}}}$, with Δ_{r} the difference between the mass of the state containing the nucleon excitation(s) and $2m_{\mathrm{N}}$. Since lattice results suggest that the lowest state with a single excitation involves the Roper resonance, whose mass is somewhat larger than the Delta, one does not expect a significant decrease in convergence rate by keeping only the nucleon explicit in the EFT.

Therefore, we formulate $\not{\pi}$EFT as an EFT formally equivalent to $\not{\pi}$EFT, but with different scales and values for the LECs. The breakdown or high-momentum scale Q_{high} is assumed to be the smallest of m_π and $\sqrt{m_{\mathrm{N}}\Delta_{\mathrm{r}}}$. The low-momentum scale Q_{low} is set by the binding momenta of the nuclei we consider and by the external momenta in the reactions we are interested in. We expand all observable in powers of $Q_{\mathrm{low}}/Q_{\mathrm{high}}$. Eventually, an NLO calculation will yield an estimate on the convergence rate and thereby the breakdown scale of $\not{\pi}$EFT. The Lagrangian in LO is given by Eq. (1), in which four m_π-dependent parameters enter: the nucleon mass m_{N} and the LECs $C_{s,t}$ and D_d.

For the calculation of few-body observables we solve the Schrödinger equation in configuration space. The potential is the sum of all irreducible contributions to the A-body scattering matrix from the Lagrangian. This amounts at LO to the sum of three tree-level diagrams with vertex factors $C_{s,t}$ and D_d. The infinities resulting from the zero-range contact interactions are here regularized via Gaussian regulator functions, $\Lambda^3 \exp(-\Lambda^2\mathbf{r}_{ij}^2/4)/(16\pi^{3/2})$ for two nucleons i,j and $\Lambda^6 \exp[-\Lambda^2(\mathbf{r}_{ik}^2 + \mathbf{r}_{jk}^2)/4]/(64\pi^3)$ for three nucleons i,j,k, where Λ *arbitrarily* separates states included explicitly as propagating degrees of freedom from states accounted for implicitly in the LECs. If it is smaller than the breakdown scale it produces larger errors than the truncation of the EFT Lagrangian (Sec. V A 2 exemplifies ramification of a violation of this condition). The resulting Schrödinger equation for the A-body wave function Ψ and the corresponding energy E takes the form

$$\left\{ -\sum_i \frac{\nabla_i^2}{2m_{\mathrm{N}}} + \sum_{i<j} \frac{1}{2} \left[C_{1,0} + C_{0,1} + (C_{1,0} - C_{0,1})\,\boldsymbol{\sigma}_i \cdot \boldsymbol{\sigma}_j \right] e^{-\frac{\Lambda^2}{4}r_{ij}^2} + \sum_{i<j<k} \sum_{cyc} D_1 e^{-\frac{\Lambda^2}{4}(r_{ik}^2 + r_{jk}^2)} \right\} \Psi = E\,\Psi. \tag{3}$$

Here, a factor from the regulator was absorbed into the bare couplings of Eq. (1):

$$C_{0,1}(\Lambda) = \frac{\Lambda^3}{16\pi^{3/2}}C_s(\Lambda), \tag{4}$$

$$C_{1,0}(\Lambda) = \frac{\Lambda^3}{16\pi^{3/2}}C_t(\Lambda), \tag{5}$$

$$D_1(\Lambda) = \left(\frac{\Lambda^3}{8\pi^{3/2}} \right)^2 D_d(\Lambda). \tag{6}$$

As in any EFT, the bare LECs depend on Λ so as to guarantee that observables do not. The Λ-dependent LECs are determined from input data in Sec. IV, after we discuss the solution of Eq. (3) in the next section.

III. TOOLBOX

To solve the Schrödinger equation we have utilized two computational methods: EIHH and $\mathbb{R}$GM. Hereafter, we present a short description of both methods.

A. The Effective-Interaction Hyperspherical Harmonics Method

The hyperspherical coordinates are the D-dimensional generalization of the 3-dimensional spherical or polar coordinates. As such they allow the description of the A-body wave function in terms of a single length variable, the

hyper-radius ρ, and $(D-1)$ *hyper*-angular variables Ω [75, 76]. Removing the center-of-mass coordinate, the A-body dynamics can be described by $A-1$ Jacobi vectors $\boldsymbol{\eta}_1, ..., \boldsymbol{\eta}_{A-1}$, therefore $D = 3A - 3$.

The nice feature of these coordinates is that, in perfect analogy to the two-particle case, the kinetic energy operator T of the A-particle system splits into a *hyper*-radial and *hyper*-centrifugal terms, with a *hyperspherical* angular momentum operator $\hat{K}$ that depends on Ω. The resulting A-particle Hamiltonian reads

$$H^{[A]} = -\frac{1}{2m_{\mathrm{N}}} \left(\Delta_\rho - \frac{\hat{K}^2}{\rho^2} \right) + V^{[A]}(\rho, \Omega) , \tag{7}$$

where Δ_ρ is the *hyper*-radial Laplacian.

The hyperspherical harmonics (HH) $\mathcal{Y}_{[K]}$ are the A-body generalization of the spherical harmonics. As such they are the eigenfunctions of $\hat{K}^2$ with eigenvalues $K(K + 3A - 5)$. They form a complete set of *hyper*-angular basis functions. Choosing a complementary set of *hyper*-radial basis states $R_n(\rho)$, the A-body wave function can be expanded in the form

$$\Psi(\rho, \Omega) = \sum_{n[K]} C_{n[K]} R_n(\rho) \mathcal{Y}_{[K]}(\Omega) \tag{8}$$

with coefficients $C_{n[K]}$. The nuclear wave function Ψ must be complemented by the spin-isospin parts, and the whole function must be antisymmetric. The construction of antisymmetric HH spin-isospin basis states is a non-trivial task, which, however, has been solved in Refs. [57, 58].

To accelerate the convergence rate of the HH expansion, Eq. (8), we construct an effective interaction (EI) using the Lee-Suzuki similarity transformation [77]. Applying the this method to the HH basis we identify the model space P with all the A-body HH states such that $K \leq K_{max}$, and the complementary space $Q = 1 - P$ as the rest of the Hilbert space. The Lee-Suzuki method then gives a recipe to construct a similarity transformation such that the spectrum of the resulting effective P-space Hamiltonian, $H^{[A]eff} = T + V^{[A]eff}$, coincides with the spectrum of $H^{[A]}$. Finding $V^{[A]eff}$, however, is as difficult as solving the original problem, and therefore we do not search for the *total* EI, but for a *partial* EI constructed through the solution of the simpler two- and three-body problems.

The resulting EI is tailored to our HH model space, and constrained to coincide with the bare one when enlarging the model space. This EIHH method [42–44] has been successfully applied to the study of bound states and reactions for nuclear systems with $3 \leq A \leq 7$.

B. The Refined Resonating-Group Method

In contrast to the EIHH method where the few-body wave function is expanded over a complete set of states, the $\mathbb{R}$GM is a variational approach that utilizes an over-complete set of states (for its original formulation, see Ref. [70, 71]; for the refinement and implementation, Ref. [69]). To construct these states, the $\mathbb{R}$GM considers all possible channels $\{[c]\}$, where each channel consists of a specific spin-isospin configuration $\Xi_{[c]}$, a set of Jacobi vectors $\boldsymbol{\eta}_1, \ldots, \boldsymbol{\eta}_{A-1}$, and the angular momentum quantum numbers $\ell_1, \ldots, \ell_{A-1}$ associated with these vectors. The orbital functions are given by the ansatz

$$R_{n[c]}(\boldsymbol{\eta}_1, \ldots, \boldsymbol{\eta}_{A-1}) = \prod_{j=1}^{A-1} \eta_j^{\ell_j} Y_{\ell_j m_j}(\hat{\eta}_j) e^{-\kappa_{nj} \eta_j^2} , \tag{9}$$

where $Y_{\ell m}$ are the spherical harmonics, and κ_{nj} are a set of width parameters used to expand the wave function, *i.e.*, the sum over the channels includes an expansion of each radial dependence in Gaussians with widths $\{\kappa_{nj}\}$.

The few-body wave function is then a linear combination of an antisymmetric product of a spin-isospin channel state and the orbital function, coupled to yield the desired total angular momentum quantum numbers JM,

$$\Psi_{JM} = \mathcal{A} \sum_{n[c]} C_{n[c]} \left[R_{n[c]} \otimes \Xi_{[c]} \right]^{JM} . \tag{10}$$

The sum over channels allows the consideration of all possible spin-isospin configurations or clusters $\Xi_{[c]}$. In practice, however, our implementation omits channels that have negligible contribution to the wave function. For example, the ansatz for the alpha-particle wave function includes triton-proton, helion-neutron, and deuteron-deuteron spin-isospin configurations. The conceivable two-neutron–two-proton arrangement was found to contribute less than 100 keV to B_α and therefore is not included in the variational ansatz.

Thus, the $\mathbb{R}$GM method includes three intertwined expansions: *i)* the cluster or resonating-group expansion, which defines the spin-isospin configuration and the Jacobi coordinates; *ii)* the partial-wave expansion; and *iii)* the expansion in Gaussian functions. Convergence is assessed along each of those "axes". First, the thresholds of a system serve as guidance for the initial choice of resonating groups. Second, contributions from subleading partial waves are considered. For *s*-wave nuclei, and central forces, $\ell > 0$ configurations do not have to be included due to the cluster expansion. Consequently, at this order of our EFT we consider only $\ell = 0$ terms in our description of the light, $A \leq 4$ nuclei. Third, the set of Gaussians is extended and scaled until this modification of the model space does not affect binding energies by more than 1%.

With the $\mathbb{R}$GM, we also calculate scattering observables. To solve the few-body problem with the $\mathbb{R}$GM for a range of cutoff (Λ as introduced above to obtain the regularized Eq. 3) values, *i.e.*, to approximate a wave function with structure around $\eta_j \approx \Lambda^{-1}$, the variational basis has to be either very large — leading to numerical instabilities— or tailored to each Λ — requiring a convergence check with regards to all parameters of the basis set.

Our variational approach is analog to Kohn-Hulthèn's method [78] which minimizes a functional parameterizing the reactance matrix, corresponding to Ricatti-Bessel asymptotic solutions for uncharged particles and Coulomb functions for charged fragments. We use in- and out-going waves as boundary conditions (spherical Hankel functions $h^{\pm}$), because this method turned out to be more accurate in practice. Specifically, for two-fragment scattering with an incoming channel c we denote the relative intercluster Jacobi coordinate by η_c and make the ansatz

$$\Psi = \mathcal{A}\left(-h_c^-(\eta_c) + \sum_{c'} S_{cc'} h_{c'}^+(\eta_{c'}) + \sum_{n[c] \in \mathcal{C}} D_{n[c]} R_{n[c]}\right), \tag{11}$$

with variational parameters $S_{cc'}$ (the S matrix) and $D_{n[c]}$. If either target or projectile are compound objects, *e.g.*, the deuteron in Sec. V A, their wave functions are predetermined via the ansatz in Eq. (10) and multiplied with the asymptotic solutions $h^{\pm}$ of the relative motion. For small distances η_c, the interaction between nucleons of different fragments is non-zero and the full scattering wave function will differ from the asymptotic form as given by the first two terms in Eq. (11). This difference is described by the third term in Eq. (11). Convergence and stability are assessed with respect to the subset $\mathcal{C}$ which is taken from the full set of channels. It is sufficient to include those $n[c]$ in $\mathcal{C}$ which are non-zero for $\eta_c \approx \Lambda^{-1}$ and, as Gaussians, square-integrable. For $\eta_c \gg \Lambda^{-1}$, this expansion should be zero, *i.e.*, Ψ is identical to the asymptotic solution. The Kohn-Hulthèn variational condition expressed in terms of the scattering matrix is

$$\delta\left\{\langle\Psi|\left(H - E_{\mathrm{c.m.}}\right)|\Psi\rangle - iS_{cc}\right\} = 0, \tag{12}$$

where $E_{\mathrm{c.m.}}$ is the center-of-momentum energy. This condition yields optimal values for $S_{cc'}$ and $D_{n[c]}$. Here the channel index c discriminates between different two-body fragmentations, *e.g.*, neutron/deuteron or neutron/neutron-proton singlet, and angular momentum. Using an appropriate decomposition of the Hamiltonian (for the latest summary and references to the original work see Ref. [82]), the variational coefficients $S_{cc'}$, $D_{n[c]}$ can be expressed in terms of integrals of the short-ranged part of the potential. Therefore, an accurate expansion of the asymptotic solution is required for a finite range. In practice, we minimize

$$I(\epsilon) = \int_0^\infty d\eta \left(h_c^{\pm}(\eta) - \sum_{n[c]} C_{n[c]} R_{n[c]}\right)^2 \eta e^{-\epsilon\eta^2}, \tag{13}$$

to approximate the Hankel or Coulomb functions. Finally, we obtain scattering lengths from the phase shift $\delta(E_{\mathrm{c.m.}})$ at a finite $E_{\mathrm{c.m.}}$ through

$$a(E_{\mathrm{c.m.}}) = -\frac{1}{k \cot \delta(E_{\mathrm{c.m.}})}. \tag{14}$$

As the scattering length is defined for $E_{\mathrm{c.m.}} = 0$, the uncertainty due to this approximation has to be assessed. In this work, we extracted a at 0.001 MeV, used 10-13 Gaussians to expand the deuteron and singlet neutron-proton fragment in the three-body scattering calculations, and adapted the Hankel functions with a weight $\epsilon = 0.03$ fm^{-2}.

To conclude, we summarize the convergence check:

- First, we determine appropriate Gaussian basis for the fragments by fixing the number of Gaussians and optimize their widths via a genetic algorithm [62].
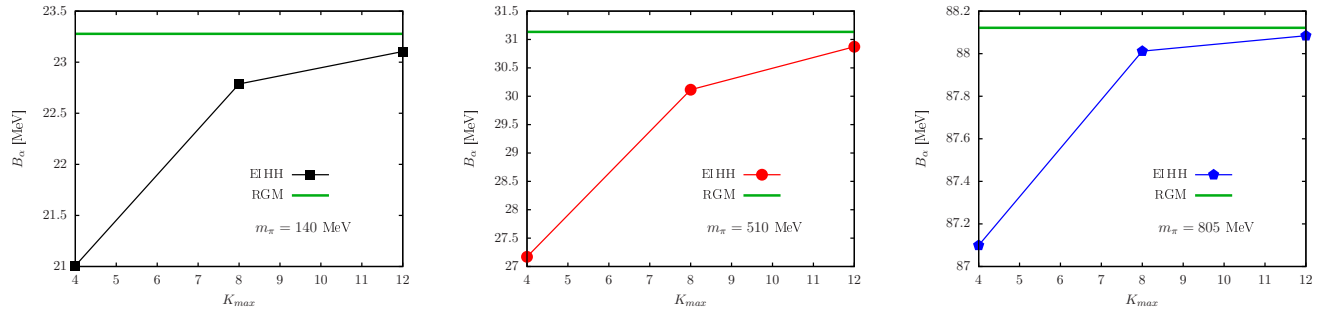
FIG. 1.   Dependence of the alpha-particle binding energy B_α (in MeV) calculated with the EIHH method on the maximal *hyper*-angular eigenvalue K_{max}. Results are shown for a $\not\pi$EFT interaction with $\Lambda = 2$ fm^{-1} at $m_\pi = 140$ MeV (left panel), 510 MeV (center), and 805 MeV (right). The horizontal green line represents the corresponding $\mathbb{R}$GM result.

- Second, we diagonalize the Hamiltonian, Eq. 3, in the scattering basis. This basis uses a different coupling scheme which adopts the one implied in Eq. (10) for each fragment. The total fragment spins are coupled to a channel spin which forms, with the orbital angular momentum on the relative coordinate η_c between the fragments, the total J. We enlarge $\mathcal{C}$ until the lowest eigenvalues reproduce the thresholds defined by the ground states of the fragments and the bound states of the compound system of the two fragments, if there is a bound state in the channel (the triton in Sec. V A).

- Third, we take

$$\lim_{\epsilon \to 0} I(\epsilon) \quad \text{and} \quad \lim_{E \to 0} a(E) \tag{15}$$

in Eqs. (13 and (14). While taking both limits, we identify a plateau in the predicted scattering length for $\epsilon < \Lambda^2$ and $E_{\text{c.m.}} < 0.0001$ MeV.

After these steps, we deem the basis large enough for an accuracy that is then dominated by the higher-order contributions of the EFT expansion.

C.   Comparison

With EFT parameters calibrated as described below, we compared the results for B_{T} and B_α of the $\mathbb{R}$GM with the corresponding EIHH values to test the accuracy of the resonating-group expansion. As an example, we show in Fig. 1 the convergence of EIHH calculations to the $\mathbb{R}$GM results for B_α at a cutoff $\Lambda = 2$ fm^{-1}. For all three pion masses, the EIHH converges with K_{max} to the respective $\mathbb{R}$GM value.

For subsequent calculations the $\mathbb{R}$GM was chosen to minimize computing time.

IV.   CALIBRATION

Through Eq. (3), all LO predictions depend on three LECs $C_{S,T}$ ($S, T = 0, 1$ or $1, 0$) and D_1, besides the nucleon mass. Lattice data are available for the two- and three-body binding energies ($B_{\text{nn}}, B_{\text{D}}, B_{\text{T}}$) at $m_\pi = 510$ MeV [38] and at $m_\pi = 805$ MeV [37]. At $m_\pi = 805$ MeV [39], the singlet and triplet scattering lengths ($^1 a_{\text{np}},^3 a_{\text{np}}$) and effective ranges are also available . We fit $C_{S,T}$ to the two-nucleon binding energies in the singlet and triplet channels ($B_{\text{nn}}, B_{\text{D}}$) by solving the Schrödinger equation via the Numerov algorithm. The D_1 term is fixed through B_{T} using the $\mathbb{R}$GM. For comparison, we also consider the physical pion mass, $m_\pi = 140$ MeV, where we fit the experimental singlet scattering length, in addition to experimental deuteron and triton binding energies.

These renormalization conditions determine the Λ dependence of the LECs. The values of the bare LECs for cutoffs $\Lambda = 2, 4, 6, 8$ fm^{-1} are given in Table II. and a graphical representation of the fit results is given in Fig. 2. The input to calibrate the values at the physical pion mass (black squares in Fig. 2), namely the deuteron binding energy and the singlet neutron-proton scattering length, are known accurately. Thus we abstain from a display of the sensitivity of those values to the uncertainty in the input. For the unphysical pion masses, the uncertainty in the input data is significant. For each cutoff, we thus obtain LECs not only for the central values but also for the boundaries of the

TABLE II. The LO LECs $C_{S,T}$ and D_1 [GeV] for real ($m_\pi = 140$ MeV) and lattice ($m_\pi = 510$, 805 MeV) nuclei for various values of the momentum cutoff Λ [fm^{-1}]. $D_1^{(*)}$ yields the triton as the ground (excited) state.

m_π	Λ	$C_{1,0}$	$C_{0,1}$	D_1	D_1^*
140	2	−0.142	−0.106	0.068	-
	4	−0.505	−0.435	0.677	-
	6	−1.09	−0.986	2.65	-
	8	−1.90	−1.76	7.82	-
510	2	−0.145	−0.130	0.157	−0.120
	4	−0.438	−0.412	0.907	−0.441
	6	−0.889	−0.853	3.21	−0.855
	8	−1.50	−1.45	9.44	−1.27
805	2	−0.148	−0.138	0.071	-
	4	−0.405	−0.388	0.354	-
	6	−0.789	−0.766	1.00	-
	8	−1.30	−1.27	2.22	-
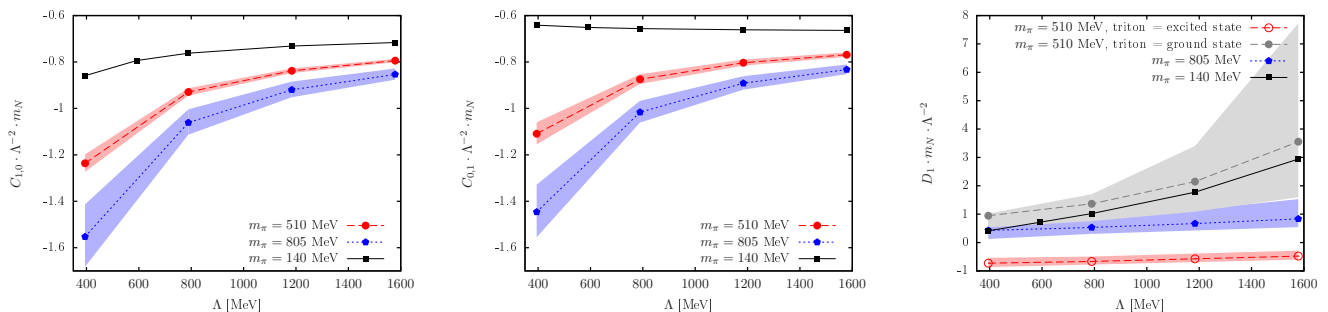
FIG. 2. Dependence on the cutoff Λ (in MeV) of the LO LECs of $\slashed{\pi}$EFT: $m_N \Lambda^{-2} C_{1,0}$ (left panel), $m_N \Lambda^{-2} C_{0,1}$ (middle), and $m_N \Lambda^{-2} D_1$ (right). The squares ($m_\pi=140$ MeV), circles (510 MeV), and pentagons (805 MeV) represent values fitted to the central values of the shallowest two-nucleon S-matrix poles in the singlet and triplet channels. D_1 is adjusted to the triton as the ground (full circles) or (for $m_\pi=510$ MeV only) first-excited (empty circles) three-nucleon state. The shaded uncertainty is obtained by varying the input data within its margin of error.

two- and three-body binding energies. In the case of D_1, we fix the two-nucleon LECs to their central values when varying B_T within its error margins. The widths of the blue ($m_\pi=805$ MeV) and red/gray (510 MeV) bands in Fig. 2 represent how input-data uncertainty translates into coupling strength uncertainty.

Some aspects of the cutoff dependence of the LECs shown in Fig. 2 can be understood from general arguments. For a non-derivative four-nucleon LEC C (multiplied by $\Lambda^3/(16\pi^{3/2})$ as in Eqs. (4) and (5)) which determines a scattering length a, an expansion in powers of relative momentum over Λ of the loop integrals appearing in the T matrix gives [66]

$$m_N \Lambda^{-2} C(\Lambda) = \theta_0 + \frac{\theta_1}{a\Lambda} + \mathcal{O}\left((a\Lambda)^{-2}\right), \tag{16}$$

where θ_i are regulator-dependent numbers of $\mathcal{O}(1)$ that depend neither on a nor on m_N, and thus also not on m_π. This large-Λ behavior is apparent in the left and middle panels of Fig. 2, where we display $m_N \Lambda^{-2} C_{S,T}$ rather than $C_{S,T}$. As we can see, all curves approach a limit $\theta_0 \simeq 0.7$, at a rate that depends on a. The different sign of the scattering length in the singlet channel for physical m_π results in a different approach to the asymptotic value compared to the other channels and pion masses, where relatively shallow bound states exist.

We can also gain some insight into the cutoff dependence of D_1. In the absence of a three-nucleon force, the triton spectrum depends sensitively on Λ, indicating a lack of renormalizability. The example of $m_\pi = 510$ MeV is shown in Fig. 3. When $D_1 = 0$, the open circles on the dotted line show an almost exponential dependence of the ground state on the cutoff. As indicated by the filled circles on another dotted line, around 1.2 GeV a second bound-state pole emerges, which also becomes increasingly more bound as the cutoff increases. The pattern repeats as the cutoff
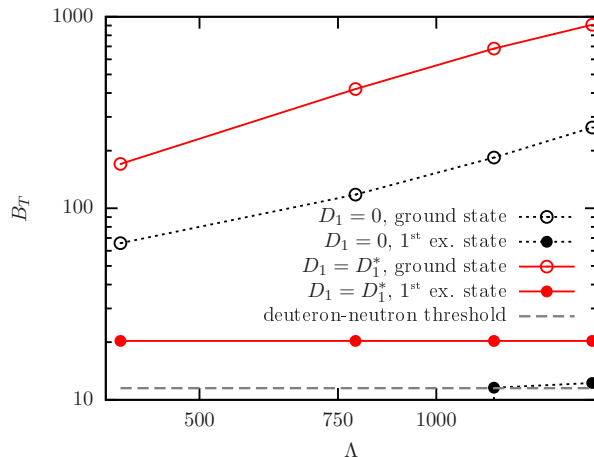
FIG. 3. Dependence on the cutoff Λ (in MeV) of the three-nucleon bound-state spectrum B_{T} (in MeV) in the triton channel at m_π=510 MeV. The neutron-deuteron threshold is indicated by a dashed line. Empty (filled) circles mark ground (excited) bound states. The dotted lines are for $D_1 = 0$. For the full lines the three-nucleon force fixes the shallow state to B_{T}.

increases further. Renormalizability can be achieved with the non-derivative three-body force [21–23]

$$m_{\mathrm{N}}\Lambda^{-2}D_1(\Lambda) = F(\Lambda/\Lambda_*)\,,\tag{17}$$

where Λ_* is an m_π-dependent parameter that determines the three-body spectrum and F is a dimensionless function that depends on the regulator and on which state is kept at the observed B_{T}. Accordingly, in the right panel of Fig. 2 we display $m_{\mathrm{N}}\Lambda^{-2}D_1$.

For all values of m_π we fit D_1 to ensure the deep bound state remains at the observed value of B_{T}, in which case F increases monotonically with Λ. The resultant values of the LEC define bands which vary significantly in width with m_π. For m_π=805 MeV (blue band around pentagons in the right panel of Fig. 2) and the physical m_π (black squares), the band width is narrow relative to m_π=510 MeV (gray band around circles). All three bands correspond to repulsive interactions. This means that without a three-nucleon force there is a three-body state which is more bound than the observed triton. This state is then "raised" to the triton by the repulsive interaction.

Since additional three-body bound-state poles appear at the two-body threshold with increasing cutoff, it is possible to renormalize D_1 to a shallow state instead. In this case, F changes. In the example of Fig. 3, we can fit $D_1(\Lambda)$ so that the first excited state is "lowered" to the triton level as indicated by the filled circles on a full line — we label the corresponding values of D_1 as D_1^* in Table II and Fig. 3. In this case, two states remain bound: the triton and a deep state shown by the empty circles on full line in Fig. 3, the latter with a binding energy that goes from 170 MeV at $\Lambda = 400$ MeV to 900 MeV at $\Lambda = 1.6$ GeV. The increased binding of the deep state compared to its binding when $D_1 = 0$ shows that the force is attractive in this range of cutoffs, and it indeed has an opposite sign to the force that keeps the ground state at B_{T}, as seen in Fig. 3.

The functional dependence of the three-nucleon LEC in Fig. 2 is, by construction, identical to that of the binding energies on the cutoff when $D_1 = 0$. The latter grows faster than quadratic (upward bending of the black dotted line with empty circles in Fig. 3). This deviation is consistent with the increase of D_1 in Fig. 2 which is not just quadratic but receives contributions from higher powers of Λ. For both fitting choices, we find the uncertainty in D_1 by taking $B_{\mathrm{T}} \in [15.8, 24.8]$ MeV (see Table I) at m_π=510 MeV. It is considerably larger when a repulsive three-nucleon force is used, as shown by the width of the gray band in the right panel of Fig. 2, which is much larger than the red band that represents the variation in the attractive force strength. In contrast to the log-periodic behavior of the three-body force as a function of the cutoff found in Refs. [21–23] we find both, the central value and the uncertainty, to increase monotonically with Λ for all m_π except for the calibration to the excited state (empty circles in Fig. 2). No discontinuities at critical values of Λ are observed because the eigenstate we chose to fit D_1 was always either the ground or the first excited state. A log-periodic F, as in Refs. [21–23], is found if the LEC is calibrated always to the shallowest state in the spectrum. As a consequence, after renormalization the smallest binding energy is fixed, while states accrete from very large binding energies at the critical values of Λ.

The significant difference in uncertainty of the three-nucleon-force parameter when fitted to the ground or excited state is related to the functional dependence of those states on Λ. In the vicinity of a critical Λ where an additional state enters the spectrum, the eigenvalue of the excited state increases much slower than that of the ground state

(compare slopes of the dotted lines in Fig. 3). The respective three-nucleon interaction strength inherits a larger slope if the ground state is fitted relative to calibrating the excited state. Since both input and regulator variation represent a change in the renormalization scheme, the observed difference in uncertainty is a consequence of the differences in slope.

Different values of Λ and different regularization schemes correspond to different models of the short-distance behavior of the theory. These models might allow for deeply bound states in the deuteron, triton, and alpha-particle spectra. A tenet of EFT is that high-energy, or short-distance, phenomena can be accounted at each order by the most general interactions consistent with symmetries and required by RG invariance. In the specific case, we use this tenet to conjecture that low-energy observables, such as the nD scattering lengths, should be independent of whether we fit the triton to the deepest, second-deepest, ..., or shallowest state. This has been seen in simple explicit examples, such as Ref. [61], where invariants of few-body spectra were analyzed with respect to changes in the short-distance structure of the employed models. It is not the scope of this work to assess differences between the various schemes, and hence we employ repulsive three-nucleon forces consistently in all calculations below.

V. RESULTS

The Phillips [33] and Tjon [11] correlations are non-trivial features of nuclear physics. Their sensitivity with respect to m_π is analyzed here. In addition, we consider the quartet three-nucleon channel which is less sensitive to the short-distance structure of the interaction, *i.e.*, no three-nucleon interaction contributes up to high order. With these predictions, we conclude that key nuclear properties are, qualitatively, insensitive to m_π — a conjecture based on the universal EFT approach. We compare the results for m_π=510 MeV and m_π=805 MeV with LO $\not\pi$EFT results at the physical pion mass to make similarities and differences explicit.

Besides identifying the peculiarities of large pion masses, we predict the outcomes of "experiments" in these hypothetical worlds. As described in the previous section, for each cutoff, *i.e.*, model for unobservable short-distance structure, $\not\pi$EFT differs in its coupling constants. If these models differ in predictions by a finite amount, it is this amount that quantifies the theoretical error. In the physical world, theoretical error estimates of this kind were used previously to make predictions through correlations (see *e.g.* Refs. [45, 46]). Since the theoretical error for B_τ and B_α is large relative to the experimental one, the Phillips and Tjon lines at LO in $\not\pi$EFT do not constrain observables further at physical m_π. At larger m_π, however, the lattice uncertainty is still significant (see Table I) and, *a priori*, there is no reason why $\not\pi$EFT should not be able to constrain observables more tightly through those correlations than solely by the "experimental" error.

We assess sensitivity of results to higher-order terms in the EFT expansion by a variation of the cutoff-regulator parameter in the range $\Lambda \in \{2, 4, 6, 8\}$ fm^{-1}. This range includes the critical value for appearance at the physical pion mass of an excited state, when $D_1 = 0$ (see discussion of Fig. 3 in Sec. IV). For lattice pion masses, the upper limit is 2-3 times the expected breakdown scale, where in general we see signs of convergence in observables. Although we might ideally want even higher cutoffs at the expense of further computational time, our estimate of the truncation error is probably not an underestimate because we include cutoff values below the expected breakdown scale. Such low cutoffs introduce larger errors than the truncation. A more reliable error estimate has to await higher-order calculations where the breakdown scale manifests itself.

A. The Three-Body Sector

The physical nucleon-deuteron system splits into two significantly different spin channels: doublet (or triton) with $s = 1/2$ and quartet with $s = 3/2$. The former (latter) supports (does not support) a bound state. In the doublet channel, an additional counterterm enters at LO — D_1 term in Eq. (3) — while the quartet channel is renormalized with $C_{S,T}$, only. The consequences to large m_π are the subject of the following two sections. Since we include no Coulomb interactions, our results at physical pion mass apply only to neutron-deuteron scattering.

1. Neutron-deuteron $^4S_{3/2}$ channel

The phase shifts in the quartet channel can be calculated in LO solely on the basis of two-nucleon input. In Fig. 4, we show our phase shift results for elastic nD scattering below 10 MeV, calculated with the $\mathbb{R}$GM. For all three pion masses, the cutoff variation between 2 fm^{-1} and 8 fm^{-1} is shown by green (m_π=140 MeV), red (m_π=510 MeV), and blue (m_π=805 MeV) bands. The upper (lower) edge corresponds to 8 (2) fm^{-1}. For the physical m_π, we compare our results to previous LO and N^{2}LO $\not\pi$EFT calculations [17, 22] (black solid and dashed-dotted lines) obtained from
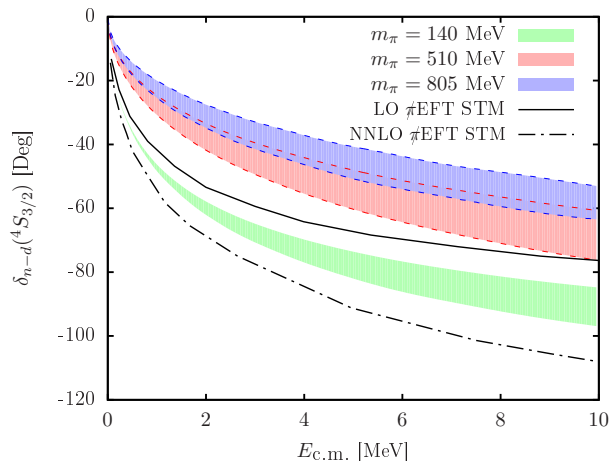
FIG. 4. Elastic neutron-deuteron scattering phase shift δ in the spin-quartet $^4S_{3/2}$ channel (in degrees) for various pion masses as function of the center-of-mass energy $E_{c.m.}$ (in MeV). The green (m_π=140 MeV), red (m_π=510 MeV), and blue (m_π=805 MeV) shaded areas are the LO $\pi\!\!\!/$EFT results of the $\mathbb{R}$GM for a cutoff in the range $[2,8]$ fm^{-1}. For the overlapping $m_\pi = 510, 805$ MeV uncertainty bands, the upper (lower) edge, corresponding to $\Lambda = 8\,(2)$ fm^{-1}, is given by dashed lines. For m_π=140 MeV, the solid (dashed-dotted) black line represents LO (N^{2}LO) $\pi\!\!\!/$EFT results from the solution of the STM equation [17, 22].
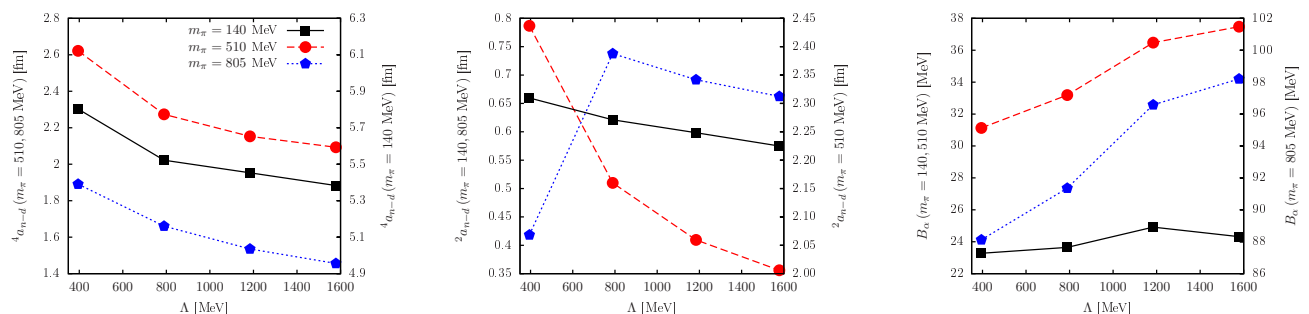

FIG. 5. Dependence on the cutoff Λ (in MeV) of the quartet ($^4a_{\text{nD}}$, left) and doublet ($^2a_{\text{nD}}$, center) neutron-deuteron scattering lengths (in fm), and of the alpha-particle binding energy B_α (right, in MeV), for $m_\pi = 140$ MeV (black squares), 510 MeV (red circles), and 805 MeV (blue pentagons).

the solution of the Skorniakov–Ter-Martirosian (STM) equations. The difference between these curves is, of course, a good reflection of the uncertainty of the LO calculation at the physical pion mass. Our result has the correct energy dependence and lies between the two curves. Our error band accounts for cutoff variation but not numerical uncertainty. The latter is included in the postdiction of the nD scattering length given below. The energy dependence and band widths are similar for the three values of the pion mass we consider. This suggests an invariance with respect to m_π of the uncertainty — and therefore the convergence rate of the EFT.

We extract a scattering length at $E_{c.m.} = 0.001$ MeV. The cutoff dependence is illustrated in the left panel of Fig. 5. For all values of the pion mass we observe a nice convergence pattern. Our final values are shown in the first row of Table III. The errors are the sum of the sensitivity to higher-order effects assessed with the cutoff variation, and the numerical uncertainty, which we measured to be less than 1 fm. They are of similar size for the three pion masses, as for the phase shifts at higher energies.

The quartet scattering length is an example of what is sometimes called a low-energy theorem: to a high order it is entirely determined by LECs fixed in other processes. The value we obtain for $^4a_{\text{nD}}$ at physical pion mass is consistent with the $\pi\!\!\!/$EFT postdictions [20] of $^4a_{\text{nD}} = 5.1 \pm 0.80$ at LO and $^4a_{\text{nD}} = 6.4 \pm 0.020$ at N^{2}LO, and with the experimental value [79]. We find a slow decrease with m_π, but no significant change, which could have arisen if there were a shallow bound state in this channel. The ERE should apply below the deuteron break-up threshold, where the deuteron can be treated as a single body. We might expect that, barring some fine-tuning, the size of the ERE parameters is set by the deuteron break-up threshold. $k_{\text{pn}} \simeq \sqrt{4m_N B_D/3}$. The numbers in Table III show indeed

TABLE III. Leading-order postdictions ($\not\pi$EFT) and predictions ($\not{\pi}$EFT) for the quartet and doublet neutron-deuteron scattering lengths $^4a_{\mathrm{nD}}$ and $^2a_{\mathrm{nD}}$ at three pion masses, in comparison with experiment and LQCD. The theoretical uncertainty considers cutoff variation between 2 fm^{-1} and 8 fm^{-1}, model-space truncation, and LQCD-input variation.

	$\not\pi$EFT	$\not{\pi}$EFT	
m_π [MeV]	140	510	805
$^4a_{\mathrm{nD}}$ [fm]	5.5 ± 1.3	2.3 ± 1.3	1.6 ± 1.3
$^2a_{\mathrm{nD}}$ [fm]	0.61 ± 0.50	2.2 ± 2.1	0.62 ± 1.0
	experiment [79]	LQCD	
$^4a_{\mathrm{nD}}$ [fm]	6.4 ± 0.020	?	?
$^2a_{\mathrm{nD}}$ [fm]	0.65 ± 0.040	?	?

very good agreement with the expectation $|^4a_{\mathrm{nD}}| = \mathcal{O}(1/k_{\mathrm{pn}})$.

Both the convergence pattern with the cutoff (reflected in error bands) and the natural size of the resulting observables suggest that $\not{\pi}$EFT behaves in similar ways to $\not\pi$EFT. There is no evidence that observables in this channel require a different treatment from an EFT point of view for the larger pion masses, *i.e.*, the same power counting is applicable.

2. Neutron-deuteron $^2S_{1/2}$ channel

As precise calculations of the three-nucleon system became possible in the late 1960s, correlations were observed among certain three-body observables calculated with a variety of potentials fitted to two-nucleon data. The best-known example is the Phillips correlation [33] between the doublet scattering length $^2a_{\mathrm{nD}}$ and the triton binding energy B_{T}. In $\not\pi$EFT these correlations are understood [21, 22] by the fact that, if the two-body input is fixed, three-body predictions in the doublet channel still depend on one parameter in LO, which determines the three-body force in Eq. (1). As this one parameter is varied, three-body observables sensitive to the LO three-body force all change in a correlated way. $\not{\pi}$EFT, by construction, predicts the correlations, and we establish here similar higher-order uncertainties for all pion masses.

Fixing the LO three-body parameter to one datum, other observables are calculated as for the quartet channel. The cutoff dependence of the doublet neutron-deuteron scattering length is shown in the middle panel of Fig. 5 in the case where the three-body parameter is determined by B_{T}, as described in Sec. IV. Again signs of convergence are visible, but not as clearly as for the quartet scattering length. The lowest cutoff of 2 fm^{-1} is not clearly above the breakdown scale at $m_\pi = 805$ MeV, and indeed it generates significant errors. Therefore, for this pion mass we consider only cutoffs 4 fm or higher in the following analysis.

One also expects the values of the doublet scattering length to be correlated with the triton binding energy. This is particularly clear when $|B_{\mathrm{T}} - B_{\mathrm{D}}| \ll B_{\mathrm{D}}$, in which case the triton can be described as a neutron-deuteron bound state and the small binding translates into $1/^2a_{\mathrm{nD}} \ll 1$. But this correlation is observed also beyond this region: in Fig. 6, the Phillips correlation is shown for the three pion masses. As the renormalization condition fixes the binding energy but does not eliminate a residual cutoff dependence, which can only be removed by higher-order interactions, the correlation is manifest as a band of finite width rather than a one-dimensional line. This width represents the theoretical error at LO $\not{\pi}$EFT. The bands were mapped out by a line for each cutoff $\Lambda \in \{2, 4, 6, 8\}$ fm^{-1}. Each such line is parametrized by a factor multiplying the three-body interaction. At $m_\pi=805$ MeV, the correlation is about to break down for the lowest cutoff, $\Lambda = 2$ fm^{-1} (blue dashed line in Fig. 6), which is another evidence that this value cannot be considered representative of the EFT truncation error.

We extract the values for $^2a_{\mathrm{nD}}$ shown in the second row of Table III. In the doublet channel, a too-small model space can be more easily detected than in the quartet channel from an under- or over-bound triton. As a consequence, the numerical $\mathbb{R}$GM uncertainty is about 0.1 fm and therefore small relative to higher-order effects which are taken as the width of the band: 0.26 fm for $m_\pi=510$ MeV, and 0.13 fm for $m_\pi=805$ MeV. The approximately constant width of the Phillips band for all three m_π suggests invariant higher-order uncertainty with increasing B_{T}. Since higher-order effects scale with momenta — those of nucleons increase in the triton as B_{T} increases — the band should intuitively widen towards larger B_{T}. In effect, lattice input uncertainty dominates the theoretical error. For the two unphysical pion masses (center and right panels), the gray-shaded areas represent data uncertainty given in Table I. The intersections of the edges of the error bands with the correlation bands define areas (gray areas bounded by horizontal dashed lines) in the $B_{\mathrm{T}} -^2a_{\mathrm{nD}}$ plane which contains pairs of values that are consistent with all other data points. The total theoretical uncertainty as estimated in Table.III includes the error in the LQCD input, 1.71 fm for
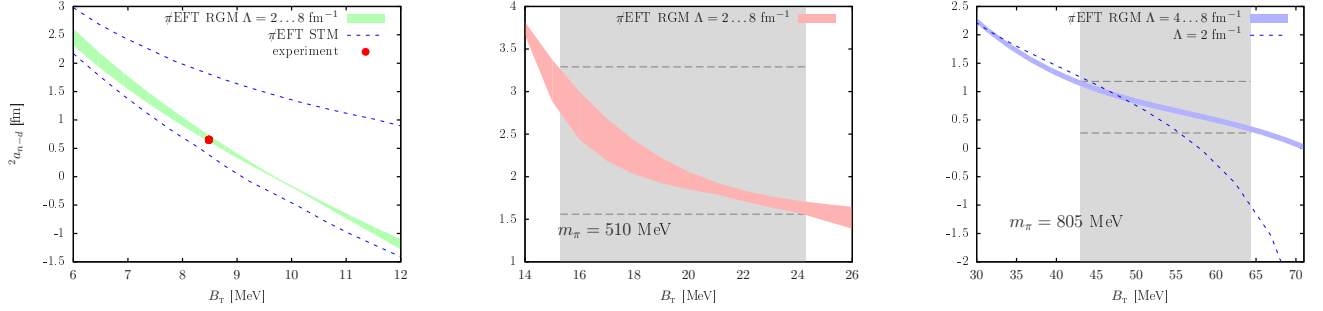
FIG. 6. Correlation between the doublet neutron-deuteron scattering length $^2a_{\mathrm{nD}}$ (in fm) and the three-nucleon binding energy B_{T} (in MeV). The green (m_π=140 MeV, left panel) and red (m_π=510 MeV, center) shaded areas are the LO $\not\pi$EFT results of the $\mathbb{R}$GM for a cutoff in the interval $[2, 8]$ fm^{-1}. The blue (m_π=805 MeV, right panel) shaded area is the LO $\not\pi$EFT results of the $\mathbb{R}$GM for a cutoff in the interval $[4, 8]$ fm^{-1}, with the cutoff $\Lambda = 2$ fm^{-1} shown as a blue dashed line. For m_π=140 MeV (left panel), experimental data are marked with a red dot and blue dashed lines display LO $\not\pi$EFT results obtained with the STM equation for sharp cutoffs of 140 and 900 MeV [16]. The gray shaded area (center and right panels) marks the lattice uncertainty in B_{T}. Values for $^2a_{\mathrm{nD}}$ between the horizontal dashed lines are consistent with all other low-energy data.

$m_\pi = 510$ MeV and 0.26 fm for $m_\pi = 805$ MeV.

The calculation at physical m_π (left panel in Fig. 6) serves as a benchmark. The dashed lines represent the solution of the STM equation at LO in $\not\pi$EFT when a sharp cutoff was varied between from 140 to 900 MeV [16]. Experiment is represented by the red dot. Our band is consistent with both. The small scattering length compared to the break-up threshold inverse momentum, $1/k_{\mathrm{pn}} \simeq 2.2$ fm, is a sign of a zero of the T matrix near the nD threshold. As discussed in Ref. [66], such a zero is located at $k_0^2 \sim -^2a_{\mathrm{nD}}\, k_{\mathrm{pn}}^3$ with respect to the origin of the complex relative-momentum plane, when $|k_0| \ll k_{\mathrm{pn}}$ and the deuteron can be treated as elementary. A consequence is a large effective range $^2r_{\mathrm{nD}} \sim -(^2a_{\mathrm{nD}}\, k_0^2)^{-1}$ and a small radius of convergence of the usual ERE. Data suggests $|k_0| \sim 20$ MeV on the imaginary momentum axis, and indeed this is what was found by explicit calculation already many years ago [80]. The negative slope of the Phillips line indicates that, as the three-body force is changed so that the triton gets more bound, this pole crosses threshold. The zero remains in the region of validity of the elementary-deuteron theory for 1 or 2 MeV around the physical value of B_{T}. In this region a modified ERE [68] holds [66].

In the center and right panels of Fig. 6) we extend LQCD to the realm of few-body scattering, which is not as easily accessible directly on the lattice. The negative slope of the Phillips line persists but the line moves up in the $B_{\mathrm{T}}-^2a_{\mathrm{nD}}$ plane, and it gets flatter, as m_π increases. The "measured" triton binding energy rises monotonously (Table I), the doublet scattering length first increases then decreases (Table III). For $m_\pi = 510, 805$ MeV, the accidental zero of the nD scattering amplitude is no longer clearly present in the region where the deuteron can be taken as elementary, and no particularly large effective range is expected.

The increasing $^2a_{\mathrm{nD}}$ with increasing B_{T} from 140 MeV to 510 MeV pion mass is opposite to the trend found for fixed pion mass, as identified above. It is not the triton binding energy but the triton-to-deuteron binding ratio shown in Table I which decreases with increasing $^2a_{\mathrm{nD}}$. This ratio is important because it measures the motion of the "experimental" point in the $B_{\mathrm{T}}-^2a_{\mathrm{nD}}$ plane: B_{D} influences (together with B_{nn}) the position of the line, and B_{T} fixes the position along the line. As the ratio $B_{\mathrm{T}}/B_{\mathrm{D}}$ decreases from m_π=140 MeV to m_π=510 MeV and increases from 510 MeV to 805 MeV pion mass, the three-nucleon bound state comes closer to and farther away from the nD threshold.

In particular, the relatively large scattering length at $m_\pi = 510$ MeV reflects a less-bound triton relative to the neutron-deuteron threshold. Once the errors are considered, B_{T} is just a few of MeV away from B_{D} at $m_\pi = 510$ MeV. In fact, in contrast to $m_\pi = 140, 805$ MeV, the binding momentum of the last nucleon can be smaller than the deuteron break-up momentum, $\kappa_{\mathrm{nD}} \simeq \sqrt{4m_{\mathrm{N}}(B_{\mathrm{T}} - B_{\mathrm{D}})/3} < k_{\mathrm{pn}}$, in which case the ERE is likely to apply. This leads to the prediction

$$^2a_{\mathrm{nD}} = \frac{1}{\kappa_{\mathrm{nD}}}\left(1 + \frac{^2r_{\mathrm{nD}}\,\kappa_{\mathrm{nD}}}{2} + \ldots\right). \tag{18}$$

The first term gives, for the central values of the binding energies, $^2a_{\mathrm{nD}} = 1.6$ fm with a correction of about 50% from the second term if $|^2r_{\mathrm{nD}}| \sim 1/k_{\mathrm{pn}}$. This estimate agrees with the central value calculated with the full three-body dynamics given in Table III. Barring significant shifts in the central values as lattice errors are reduced, in this lattice world the triton can be viewed as a two-body halo system.
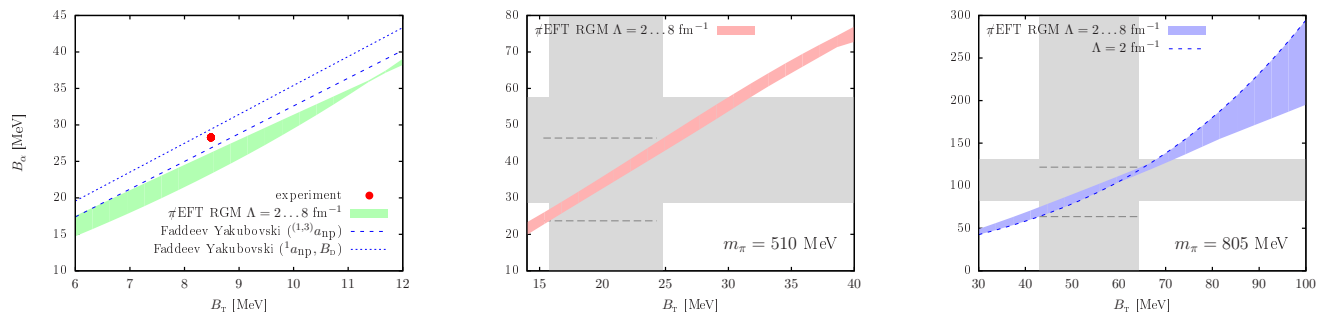
FIG. 7. Correlation between the three- (B_{T}, in MeV) and four- (B_α, in MeV) nucleon binding energies. The green (m_π=140 MeV, left panel), red (m_π=510 MeV, center panel) and blue (m_π=805 MeV, right) shaded areas are the $\mathbb{R}$GM-LO $\not\pi$EFT results for a cutoff in the interval $[2,8]$ fm^{-1}. For m_π=140 MeV (left panel), the green uncertainty band represents sensitivity to the cutoff *and* to the renormalization input (whether B_{D} or $^3a_{\mathrm{np}}$). Experimental data are marked with a red dot, and the blue dotted (dashed) line represents LO $\not\pi$EFT results from Ref. [29] using $^1a_{\mathrm{np}}, ^3a_{\mathrm{np}}$ ($^1a_{\mathrm{np}}, B_{\mathrm{D}}$) as input. The gray shaded areas in the center and right panels mark lattice uncertainty in B_{T} and B_α. Values for B_α between the horizontal dashed lines are consistent with all other low-energy data.

It is an open question whether there is a pion mass, possibly around 510 MeV, where the triton converges to the deuteron threshold. If there is, we would be witnessing a qualitatively new phenomenon in few-nucleon physics. The Efimov effect in the three-body system is a prominent example of universal feature emergent from the unitary limit in the two-body sector. A pion mass which produces the analog three-body unitarity, $1/^2a_{\mathrm{nD}} \to 0$, would be a world where the four-body system exhibits an Efimov-type spectrum.

B. The Four-Body Sector

While there is no lattice data on three-nucleon scattering observables and thus the results presented in the previous subsection remain to be verified "experimentally", *i.e.*, with a direct LQCD calculation, there is data on the ground-state energy of the four-nucleon system. In this section, we find the three- and four-nucleon ground-state energies correlated for all three m_π. At the physical m_π, the relation is known as the Tjon line [11] which can again be explained by a variation in the single LO three-body force parameter.

In Fig. 7, the correlations between the ground-state energies of the three- and four-nucleon systems are shown. The different graphs represent results for the three pion masses. We observe an increase in alpha-particle binding in step with the increase in triton binding energy, which is not surprising in pionless EFT because with fixed two-nucleon input it is the same three-body force that controls the binding of the three- and four-nucleon systems. The correlation is manifest in a band, not a line, and the width of the band measures the theoretical uncertainty assessed via cutoff variation. With the central value of B_{T} as input in the three-body force, the dependence on the cutoff of the alpha-particle binding energy B_α is shown on the right panel of Fig. 5. The slope of the correlation *lines* — as before, each line is parametrized by a variation of the D_1 three-body interaction strength — further affects the LO $\not\pi$EFT uncertainty. The larger the slope, the larger the uncertainty in B_α due to the uncertainty in B_{T}.

For the physical pion mass, our error band does not agree well with the LO results of Ref. [29] shown in the left panel of Fig. 7. In Ref. [29] the alpha-particle binding energy was found by a solution of the Faddeev-Yakubovski integral equations with a Gaussian regulator on the relative incoming (p') and outgoing (p) momenta, $\exp[-(p^2+p'^2)/\Lambda^2]$. The uncertainty was assessed by a cutoff variation $\Lambda \in [8,10]$ fm^{-1}, thus excluding a reported stronger cutoff dependence for $\Lambda < 8$ fm^{-1}. The cutoff variation was then deemed small compared to the higher-order uncertainty estimated by changing the two-body input: the two curves obtained from B_{D} and $^3a_{\mathrm{np}}$ are represented by the blue lines in Fig. 7. We have similarly examined the input dependence: for $\Lambda = 8$ fm^{-1}, we replaced B_{D} with $^3a_{\mathrm{np}}$ and found B_α (upper bound of the correlation band for m_π=140 MeV, green area, left panel in Fig. 7) larger by 2 MeV. Even with this extended variation of the renormalization scheme, the two uncertainty bands do not overlap. In contrast, the current $\mathbb{R}$GM results for the Tjon correlation band are consistent with the previous $\mathbb{R}$GM LO-$\not\pi$EFT calculation of Ref. [32]. The convergence of B_α to the physical value when the NLO potential is iterated [32] suggests that in both LO calculations the theoretical error as shown by the band widths in Fig. 7 is a lower bound. For our theoretical error estimates, we interpret $\mathbb{R}$GM and Faddeev calculations, *i.e.*, different regularizations and model-space cutoffs, as different renormalization schemes. For B_α and physical m_π, the uncertainty is thus given by the spread of results of both methods (difference between short-dashed blue line and lower edge of the green band).

TABLE IV. Predictions for the four-nucleon binding energy B_α and the universal alpha-to-triton ratio $B_\alpha/B_{\rm T}$ from LO pionless EFT at three pion masses, in comparison with experiment and LQCD. The theoretical errors include numerical and EFT uncertainty. The uncertainty in the fractions (lines 2 and 4) adds independent errors in quadrature.

m_π [MeV]	140	510	805
	$\pi\!\!\!/$EFT	$\vec{\pi}\!\!\!/$EFT	
B_α [MeV]	24.9 ± 4.3	35 ± 22	94 ± 45
$B_\alpha/B_{\rm T}$	2.9 ± 0.51	1.7 ± 1.1	1.8 ± 0.9
	experiment	LQCD	
B_α [MeV]	28.3	43.0 ± 14.4	107.0 ± 24.2
$B_\alpha/B_{\rm T}$	3.34	2.1 ± 0.85	2.0 ± 0.6

For unphysical pion masses we indicate, as before, the uncertainty in LQCD energies by gray bands in the center and right panels of Fig. 7: a vertical band for $B_{\rm T}$ and a horizontal band for B_α. Values for B_α in an interval bounded by the intersection of the upper (lower) edge of the $\vec{\pi}\!\!\!/$EFT uncertainty band with the right (left) boundary of the band of LQCD-allowed $B_{\rm T}$ values are indicated by horizontal dashed lines. This range is slightly larger than the constraint already given by "experiment" for m_π=805 MeV, and slightly narrower for m_π=510 MeV. However, given the renormalization-input dependence seen at physical pion mass, we estimate the theoretical uncertainty by conservatively doubling the width of the $\mathbb{R}$GM correlation band, plus 2 MeV as an upper bound of the numerical uncertainty (see Fig. 1 for this estimate), plus the experimental LQCD uncertainties in B_α.

The results for the alpha-particle binding energy are summarized in Table IV. The predicted value is taken as the central value in the uncertainty band. The EFT results—absolute binding energies and the ratios—are consistent with experiment at physical pion mass and with LQCD at higher masses given the uncertainty estimates on both, experimental and theoretical side. One should keep in mind that the experimental number reflects the additional effects of the Coulomb interaction between protons, which does not enter the LQCD results. As discussed in Sect. II, Coulomb effects should be of higher order in the relatively tight helion and alpha-particle ground states.

As expected, the $B_\alpha - B_{\rm T}$ correlation has a positive slope for any pion mass. For each correlation band, we define the slope with a linear regression through the $B_{\rm T}, B_\alpha$ pairs predicted with $\vec{\pi}\!\!\!/$EFT for all cutoff values which are within data uncertainty (gray areas) only. At physical m_π, our calculation yields a smaller slope (≈ 3.6) than Ref. [29] (≈ 3.8). With increasing m_π, the slope is found to decrease, ≈ 2.1 for m_π=510 MeV and m_π=805 MeV. In other words, the ratio $B_\alpha/B_{\rm T}$ *does* change with m_π, consistent with the lattice extractions, as shown in Table IV.

Since in obtaining the Tjon line the three-body force is being varied, the structure of the line (slope, curvature, intercept) must depend on the two-nucleon interactions. Indeed, from the ratios listed in Table IV we infer that whatever leads to the different ratios between the deeper two-nucleon state — recall that for unphysical masses, the interaction in the $^1S_0$ channel sustains a bound state, see Table I — and the triton is not the main factor behind the change in the slope of the Tjon line. As for the Phillips line, the structure of the Tjon line depends on both pieces of two-nucleon input. For example, in Fig. 8, we demonstrate the sensitivity of the slope of the Tjon line with respect to the pole in the spin-singlet two-nucleon amplitude. The triplet binding energy, *i.e.*, the deuteron was held fixed to the lattice central value at m_π=510 MeV , $B_{\rm D} = 11.5$ MeV. Three cases are shown for $\Lambda = 4$ fm^{-1}, corresponding to different calibrations of $C_{0,1}$, the LEC controlling the channel: *i)* a singlet neutron-proton state with binding energy of approximately 11.5 MeV, *i.e.*, the deuteron energy; *ii)* a shallow bound singlet state of $B_{\rm D} \approx 0.5$ MeV; and *iii)* an unbound singlet state. Within the considered range for $B_{\rm T}$ a linear regression to the dependence of B_α on $B_{\rm T}$ is appropriate. When the singlet two-nucleon state is very close to threshold, the slope is found maximal, $\Delta B_\alpha/\Delta B_{\rm T} \approx 3.0$ (red dashed line in Fig. 8). If the interaction is tuned away from this critical point, either to produce no bound singlet (red dotted line), or a state with identical binding energy to the triplet (red solid line), the slope parameter decreases. Naïvely, one might have expected a monotonic dependence of the slope on the strength of the two-body attraction. A larger two-body attraction requires a more repulsive three-body force to fix the triton. The contribution of this extra repulsion should be stronger in the four-particle system and hence the latter should not be as deeply bound. The non-monotonicity found above remains to be explained in a more general context taking into account the possibility of a four-body Efimov effect mentioned at the end of Sec. V A 2.

VI. CONCLUSION

We have adapted pionless effective field theory, $\pi\!\!\!/$EFT, to describe LQCD data at unphysical pion masses, dubbing it $\vec{\pi}\!\!\!/$EFT. For the first time predictions were made for a nuclear reaction, nucleon-deuteron scattering, in lattice
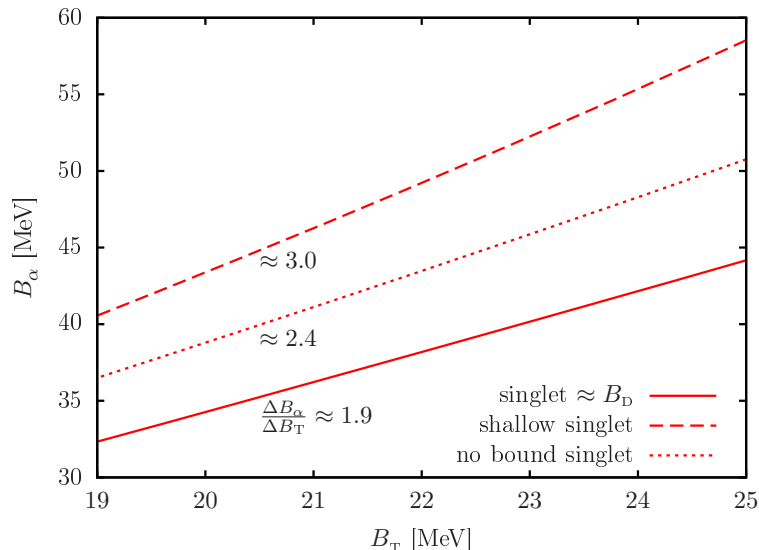
FIG. 8. Correlation between the three- (B_T, in MeV) and four- (B_α, in MeV) nucleon binding energies (Tjon line) for three values of the binding energy of the singlet two-nucleon state: same as the deuteron binding energy (continuous line, slope ≈ 1.9); shallower than the deuteron (dashed line, slope ≈ 3.0); and unbound (dashed line, slope ≈ 2.4). Results were obtained for ten values of the three-body interaction strength at $\Lambda = 4$ fm^{-1} for $B_D = 11.5$ MeV (m_π=510 MeV).

worlds where the pion mass is 510 and 805 MeV. Furthermore, the Phillips and Tjon correlations were obtained at these high pion masses with leading-order uncertainties of similar size and thus offer no indication of a significantly different convergence rate of the respective EFT expansions. The alpha-particle binding energy was found in good agreement with direct lattice measurements, which reassures us of the applicability of $\pi\!\!\!/$EFT. It also strengthens confidence in the LQCD results [37, 38] themselves, despite the apparent subtlety in identifying energy plateaus in the data.

Our work thus suggests that $\pi\!\!\!/$EFT applies to light nuclei independently of the exact LQCD data used as input. The calculations presented here could be repeated if those values change or if new values of the pion mass are explored. While this manuscript was being written, new data have appeared for $m_\pi = 300$ MeV [60], which do not quite fit with the trend of increasing binding with pion mass but show a pattern of dependence on A similar to the one found at higher pion masses [37, 38] [1]. More problematic is that another lattice collaboration [59] does not find bound states over a wide range of pion masses. Because the latter lattice data are processed through an (unobservable) potential, uncontrolled errors are introduced. Still, it is prudent to consider the specific numbers available from LQCD so far as illustrative only, and focus instead on the qualitative insights they bring into nuclear physics [2].

While much of the underlying structure of light nuclei seems to remain the same at unphysical pion mass, existing LQCD data give some hints of subtle changes. In the studied lattice worlds, the triton and alpha-particle binding energies are larger than in the real world, but their ratios to the deuteron binding energy become smaller. In contrast to the quartet neutron-deuteron channel, where we detected no qualitative changes, the accidental zero of the doublet T matrix that exists for physical pion mass near threshold seems to disappear. It is replaced by effective-range parameters that suggest a more prominent neutron-deuteron halo character for the triton. LQCD data with smaller errors, and at other values of the pion mass, would allow firmer conclusions about the organization of nucleons in the triton and its implications for the alpha particle.

In an upcoming project, NLO calculations will assess the convergence rate and breakdown scale of the EFT. They will also reduce some of the uncertainties in the extrapolation of LQCD data. In the longer term, the application of $\pi\!\!\!/$EFT to systems with more than four nucleons could guide the lattice effort to the relevant few-body observables to be measured in order to pin down additional LECs needed to understand nuclear structure.

————

[1] Note that the central values for deuteron and triton energies [60] suggest a triton with a last nucleon that is even less bound than at $m_\pi = 510$ MeV. From Eq. 18 we then expect $^2a_{nD} \simeq 2$ fm with a correction from the effective range of perhaps 40%. Alas, in this lattice world, too, the large lattice errors do not yet allow firm conclusions about the two-body halo character of triton.

ACKNOWLEDGMENTS

---

[1] S. R. Beane, W. Detmold, K. Orginos and M. J. Savage, Prog. Part. Nucl. Phys. **66**, 1 (2011) [arXiv:1004.2935 [hep-lat]].
[2] N. Barnea, L. Contessi, D. Gazit, F. Pederiva and U. van Kolck, Phys. Rev. Lett. **114**, no. 5, 052501 (2015) [arXiv:1311.4966 [nucl-th]].
[3] S. Weinberg, Physica A **96**, 327 (1979).
[4] R. A. Briceno, Z. Davoudi, T. C. Luu and M. J. Savage, Phys. Rev. D **89**, no. 7, 074509 (2014) [arXiv:1311.7686 [hep-lat]].
[5] E. Oset, H. Toki, M. Mizobe and T. T. Takahashi, Prog. Theor. Phys. **103**, 351 (2000) [nucl-th/0011008].
[6] E. E. Jenkins, Nucl. Phys. B **368**, 190 (1992).
[7] S. R. Beane, P. F. Bedaque, M. J. Savage and U. van Kolck, Nucl. Phys. A **700**, 377 (2002) [nucl-th/0104030].
[8] J. Gasser and H. Leutwyler, Annals Phys. **158**, 142 (1984).
[9] M. Pavon Valderrama and E. Ruiz Arriola, Phys. Lett. B **580**, 149 (2004) [nucl-th/0306069].
[10] M. Pavon Valderrama and E. Ruiz Arriola, Phys. Rev. C **70**, 044006 (2004) [nucl-th/0405057].
[11] J. A. Tjon, Phys. Lett. B **56**, 217 (1975).
[12] C. Thomas, PoS LATTICE **2013**, 003 (2014).
[13] J. W. Chen, G. Rupak and M. J. Savage, Nucl. Phys. A **653**, 386 (1999) [nucl-th/9902056].
[14] M. J. Savage, In *Seattle 1999, Nuclear physics with effective field theory* 136-162 [nucl-th/9905009].
[15] U. van Kolck, Nucl. Phys. A **631**, 56C (1998) [hep-ph/9707228].
[16] H. W. Grießhammer, Nucl. Phys. A **744**, 192 (2004) [nucl-th/0404073].
[17] P. F. Bedaque and H. W. Grießhammer, Nucl. Phys. A **671**, 357 (2000) [nucl-th/9907077].
[18] P. F. Bedaque, H. W. Hammer and U. van Kolck, Phys. Rev. C **58**, 641 (1998) [nucl-th/9802057].
[19] J. Vanasse, Phys. Rev. C **88**, no. 4, 044001 (2013) [arXiv:1305.0283 [nucl-th]].
[20] P. F. Bedaque and U. van Kolck, Phys. Lett. B **428**, 221 (1998) [nucl-th/9710073].
[21] P. F. Bedaque, H. W. Hammer and U. van Kolck, Phys. Rev. Lett. **82**, 463 (1999) [nucl-th/9809025].
[22] P. F. Bedaque, H. W. Hammer and U. van Kolck, Nucl. Phys. A **646**, 444 (1999) [nucl-th/9811046].
[23] P. F. Bedaque, H. W. Hammer and U. van Kolck, Nucl. Phys. A **676**, 357 (2000) [nucl-th/9906032].
[24] P. F. Bedaque, G. Rupak, H. W. Grießhammer and H. W. Hammer, Nucl. Phys. A **714**, 589 (2003) [nucl-th/0207034].
[25] H. W. Grießhammer, Nucl. Phys. A **760**, 110 (2005) [nucl-th/0502039].
[26] S. i. Ando and M. C. Birse, J. Phys. G **37**, 105108 (2010) [arXiv:1003.4383 [nucl-th]].
[27] C. Ji and D. R. Phillips, Few Body Syst. **54**, 2317 (2013) [arXiv:1212.1845 [nucl-th]].
[28] J. Vanasse, D. A. Egolf, J. Kerin, S. König and R. P. Springer, Phys. Rev. C **89**, no. 6, 064003 (2014) [arXiv:1402.5441 [nucl-th]].
[29] L. Platter, H.-W. Hammer and U. G. Meißner, Phys. Lett. B **607**, 254 (2005) [nucl-th/0409040].
[30] L. Platter, H. W. Hammer and U. G. Meißner, Phys. Rev. A **70**, 052101 (2004) [cond-mat/0404313].
[31] H.-W. Hammer and L. Platter, Eur. Phys. J. A **32**, 113 (2007) [nucl-th/0610105].
[32] J. Kirscher, H. W. Grießhammer, D. Shukla and H. M. Hofmann, Eur. Phys. J. A **44**, 239 (2010) [arXiv:0903.5538 [nucl-th]].
[33] A. C. Phillips, Nucl. Phys. A **107**, 209 (1968).
[34] F. Gabbiani, P. F. Bedaque and H. W. Grießhammer, Nucl. Phys. A **675**, 601 (2000) [nucl-th/9911034].
[35] I. Stetcu, B. R. Barrett and U. van Kolck, Phys. Lett. B **653**, 358 (2007) [nucl-th/0609023].
[36] J. Kirscher, Phys. Lett. B **721**, 335 (2013) [arXiv:1105.3763 [nucl-th]].
[37] S. R. Beane *et al.* [NPLQCD Collaboration], Phys. Rev. D **87**, no. 3, 034506 (2013) [arXiv:1206.5219 [hep-lat]].
[38] T. Yamazaki, K. i. Ishikawa, Y. Kuramashi and A. Ukawa, Phys. Rev. D **86**, 074514 (2012) [arXiv:1207.4277 [hep-lat]].
[39] S. R. Beane *et al.* [NPLQCD Collaboration], Phys. Rev. C **88**, no. 2, 024003 (2013) [arXiv:1301.5790 [hep-lat]].
[40] S. Kreuzer and H.-W. Hammer, Phys. Lett. B **673**, 260 (2009) [arXiv:0811.0159 [nucl-th]].
[41] S. R. Beane, E. Chang, W. Detmold, K. Orginos, A. Parreo, M. J. Savage and B. C. Tiburzi, arXiv:1505.02422 [hep-lat].
[42] N. Barnea, W. Leidemann and G. Orlandini, Phys. Rev. C **81**, 064001 (2010).
[43] N. Barnea, W. Leidemann and G. Orlandini, Nucl. Phys. A **693**, 565 (2001) [nucl-th/0101050].
[44] N. Barnea, W. Leidemann and G. Orlandini, Phys. Rev. C **61**, 054001 (2000) [nucl-th/9910062].
[45] J. Kirscher and D. R. Phillips, Phys. Rev. C **84**, 054004 (2011) [arXiv:1106.3171 [nucl-th]].
[46] H. W. Hammer and S. König, Phys. Lett. B **736**, 208 (2014) [arXiv:1406.1359 [nucl-th]].
[47] P. F. Bedaque and U. van Kolck, Ann. Rev. Nucl. Part. Sci. **52**, 339 (2002) [nucl-th/0203055].
[48] L. Platter, Few Body Syst. **46**, 139 (2009) [arXiv:0904.2227 [nucl-th]].
[49] D. R. Phillips, Czech. J. Phys. **52**, B49 (2002) [nucl-th/0203040].

[50] A. V. Anisovich, A. Sarantsev, O. Bartholomy, E. Klempt, V. A. Nikonov and U. Thoma, Eur. Phys. J. A **25**, 427 (2005) [hep-ex/0506010].

[51] D. B. Leinweber, A. W. Thomas, K. Tsushima and S. V. Wright, Phys. Rev. D **61**, 074502 (2000) [hep-lat/9906027].

[52] G. L. Greene, E. G. Kessler, R. D. Deslattes and H. Boerner, Phys. Rev. Lett. **56**, 819 (1986).

[53] O. Dumbrajs, R. Koch, H. Pilkuhn, G. c. Oades, H. Behrens, J. j. De Swart and P. Kroll, Nucl. Phys. B **216**, 277 (1983).

[54] M. J. Savage, Phys. Rev. C **55**, 2185 (1997) [nucl-th/9611022].

[55] T. D. Cohen, B. A. Gelman and U. van Kolck, Phys. Lett. B **588**, 57 (2004) [nucl-th/0402054].

[56] M. P. Valderrama and E. R. Arriola, Phys. Rev. C **74**, 064004 (2006) [nucl-th/0507075].

[57] N. Barnea and A. Novoselsky, Phys. Rev. A **57**, 48 (1998).

[58] N. Barnea and A. Novoselsky, Ann. Phys. (N.Y.), **256**, 192 (1997).

[59] T. Inoue *et al.* [HAL QCD Collaboration], Nucl. Phys. A **881**, 28 (2012) [arXiv:1112.5926 [hep-lat]].

[60] T. Yamazaki, K. i. Ishikawa, Y. Kuramashi and A. Ukawa, arXiv:1502.04182 [hep-lat].

[61] S. Nakaichi-Maeda, Phys. Rev. C **51**, 1633 (1995).

[62] C. Winkler and H. M. Hofmann, Phys. Rev. C **55**, 684 (1997) [nucl-th/9412032].

[63] A. Nogga, R. G. E. Timmermans and U. van Kolck, Phys. Rev. C **72**, 054006 (2005) [nucl-th/0506005].

[64] S. Durr, arXiv (2014) [hep-lat/1412.6434].

[65] D. B. Kaplan, M. J. Savage and M. B. Wise, Phys. Lett. B **424**, 390-396 (1998) [nucl-th/9801034].

[66] U. van Kolck, Nucl. Phys. A **645**, 273-302 (1999) [nucl-th/9808007].

[67] X. Kong and F. Ravndal, Nucl. Phys. A **665**, 137-163 (2000) [hep-ph/9903523].

[68] W. T. H. van Oers and J. D. Seagrave, Phys. Lett. B **24**, 562 (1967) [nucl-th/9801034].

[69] H. M. Hofmann, Proc. of Models and Methods in Few-Body Physics Lisboa, Portugal, 243 (1986).

[70] J. A. Wheeler, Phys. Rev. **52**, 1083 (1937).

[71] J. A. Wheeler, Phys. Rev. **52**, 1107 (1937).

[72] K. A. Olive *et al.* [Particle Data Group Collaboration], Chin. Phys. C **38**, 090001 (2014).

[73] A. H. Wapstra and G. Audi, Nucl. Phys. A **432**, 1 (1985).

[74] P. J. Mohr, B. N. Taylor and D. B. Newell, Rev. Mod. Phys. **84**, 1527 (2012) [arXiv:1203.5425 [physics.atom-ph]].

[75] M. Viviani, A. Kievsky and S. Rosati, Few Body Syst. **18**, 25 (1995).

[76] W. Oehm, S. A. Sofianos, H. Fiedeley and M. Fabre de la Ripelle, Phys. Rev. C **42**, 2322 (1990).

[77] K. Suzuki and S. Y. Lee, Prog. Theor. Phys. **64**, 2091 (1980).

[78] W. Kohn, Phys. Rev. **74**, 1763 (1948).

[79] W. Dilg, L. Koester and W. Nistler, Phys. Lett. B **36**, 3 208-210 (1971).

[80] J. S. Whiting and M. G. Fuda, Phys. Rev. C **14**, 18 (1976).

[81] A. Deltuva, A. Lazauskas and L. Platter, Few-Body Syst. **51**, 235-247 (2011).

[82] J. Kirscher, arXiv:1506.00347 [nucl-th].